https://doi.org/10.1016/j.trgeo.2020.100479



# Effect of strain rate on the adhesive bond shearing resistance of stiff clay

Jian HAN[1], Zhen-Yu YIN[2,*], Christophe DANO[3] and Pierre-Yves HICHER[4]

[1] School of Materials Science and Mechanical Engineering, Beijing Technology and Business University, Beijing, China

[2] Department of Civil and Environmental Engineering, The Hong Kong Polytechnic University, Hung Hom, Kowloon, Hong Kong

[3] 3SR Laboratory, Grenoble Alpes University, CNRS, Grenoble INP, Grenoble, France

[4] Research Institute of Civil Engineering and Mechanics (GeM), UMR CNRS 6183, Ecole Centrale de Nantes, Nantes, France

[*] Corresponding author: Dr Zhen-Yu Yin, Tel. +852 34008470, Fax +852 23346389, Email: zhenyu.yin@polyu.edu.hk; zhenyu.yin@gmail.com

**Abstract:** Up to now, the effect of strain rate on the adhesive bond shearing resistance of stiff clay, which plays a fundamental role in constitutive modeling of such kind of soils, remains unclear. This paper aims to experimentally investigate the strain rate dependency of the adhesive bond shearing resistance of stiff clay. Both undisturbed and reconstituted overconsolidated samples of Merville stiff clay from the Flanders region in the north of France are prepared with different overconsolidation ratios (OCR, up to 56). Oedometer tests and undrained triaxial tests under different confining stresses on samples with different OCRs are conducted. The effect of inter-particle bond is gradually investigated by comparing test results of undisturbed and reconstituted samples with the same OCR. All results suggest a uniqueness of the strain rate dependency in one-dimensional and triaxial conditions with different OCRs for the reconstituted clay, whereas the strain rate dependency of shear strength of overconsolidated clay is found to be higher in undisturbed samples than in reconstituted samples due to inter-particle bonding. This new finding is formulated as the adhesive bond shearing resistance against the strain rate, which should be useful for improving the time-dependent modeling of highly overconsolidated stiff clays.

**Keywords:** clay, viscoplasticity, rate-dependency, inter-particle bond, constitutive relation, laboratory test

# 1 Introduction

The construction of transportation infrastructure in clay regions has been increasingly developing (Gu et al., 2020; Indraratna et al., 2020). The rate-dependent behavior and strength of clay has to be carefully considered in engineering analysis and design (Yang et al., 2020; Yao et al., 2019). It is well recognized that undrained shear strength and preconsolidation pressure decrease with decreasing strain rate for normally consolidated or slightly overconsolidated soft clays (Tavenas and Leroueil, 1977; Graham et al., 1983; Zhu and Yin, 2000; Yin and Hicher, 2008; Karstunen and Yin, 2010; Yao et al., 2009; Yao et al., 2015). For overconsolidated clays, comprehensive studies on mechanical behaviors of remolded clay have been made by Sheahan et al. (1999) and Zhu and Yin (2000), with overconsolidation ratios (OCR) up to 8. Laboratory tests on London clay with different strain rates have been conducted by Sorensen et al. (2007), but without investigating the influence of heavily OCR on the rate dependent strength of stiff clay. D'Onofrio et al. (1999) studied only the rate-dependent stiffness of stiff clay. Vaid et al. (1979) studied the rate-dependent strength of intact samples under only one confining stress, which is not enough for investigating OCR and soil structure effects. For heavily overconsolidated stiff clays, the time-dependent behavior is generally assumed to be insignificant, but a lack of experimental test results can also be noted. In particular, the effect of strain rate on the adhesive bond shearing resistance of stiff clay, which plays a fundamental role in constitutive modeling of such kind of soils, has never been investigated. Note that the adhesive bond refers to the inter-particle bonding that sticks two particles and thus gives adhesive force between particles.

Therefore, progress in understanding and quantifying strain rate effects on clay behavior in undrained conditions requires additional comprehensive data on heavily overconsolidated stiff clays. This paper focuses on the strain rate dependency of the adhesive bond shearing resistance of stiff clay. Both undisturbed and reconstituted samples of Merville stiff clay are prepared. Oedometer and isotropically consolidated undrained triaxial tests under different confining stresses are conducted with different strain rates. The strain rate effect on the adhesive bond shearing resistance is investigated by comparing test results on undisturbed

and reconstituted samples.

# 2 Merville clay and test program

## 2.1 Description of Merville clay

The Merville clay from the Flanders regions in the north of France (Figure 1) was selected for the experimental study. According to the previous study (Josseaume et al., 1991), the Merville clay is of marine origin. It was deposited during the Ypresian in a marine gulf stretching across the whole area which is now located in northern France, Belgium and southeastern England. Thus, Merville clay has characteristics similar to London clay. The clay layer was then covered by tertiary sedimentation which continued until the Pliocene. The soil surface stood then probably about 200 m above the present surface of the clay. The formations overlying the clay and the top of the clay layer were later eroded. This erosion process was sustained to Quaternary by the deposition of the Flandrian alluvial deposits. The clay layer has at the present time an effective vertical stress much lower than that existing during the Pliocene. Hence, the clay is known as a stiff, heavily overconsolidated clay (Josseaume, 1998; Hieng, 1991). It presents also fissures in its top part according to the process of sedimentation-erosion over time.

As shown in Figure 1, silts of low to medium plasticity are found at the test site to a depth of about 2.4 m underlain by a highly plastic overconsolidated clay layer (Ali et al., 2010). The Merville clay used in this study is located beneath the depth of 2.4 m in agreement with previous studies (Ali et al., 2010; Canépa et al., 2002; Ferber and Abraham, 2002). The water table (WT) is located at the interface between silt and clay at about 2.4 m below the ground level in Figure 1.

The samples were retrieved from continuously sampled rotary boreholes at Merville. The stratigraphy of the site constitutes about 2.4 m of silts overlying Merville clay. The boreholes extended from the ground to about 11 m depth. Samples that were badly disturbed due to drilling were rejected and the good quality samples were stored in 1-meter long thin-wall PVC tubes. The inner diameter of the tubes is 11 cm. The rotary core samples had a circular shape, with diameter of 11 cm. They were trimmed to conventional dimensions of 35

mm in diameter and 70 mm in height. In order to obtain specimens, the initial dimension of the core was first reduced to a diameter of roughly 55 mm using sharp knives, the required dimension was achieved by using a hand lathe, a frame and trimming saws. Once the sample had been trimmed to the correct shape, it was weighed and its dimensions were accurately measured. In the thesis of Gasparre (2005), a maximum time of 20 minutes was spent trimming rotary core samples, with experience, which was enough to avoid significant drying of the London clay samples. This method was fully applied to the preparation of the specimens of Merville stiff clay. The selected undisturbed samples were sampled at depths between 9 m and 11 m. The main physical properties are summarized in Table 1. The clay can be classified as a highly plastic inorganic clay according to Casagrande's plasticity chart. After drying and grinding the clay samples to obtain a dry powder, the grain size distribution was measured as shown in Figure 2, indicating that the tested soil is a silty clay. Scanning electron microscopy (SEM) photographs were taken on samples of the undisturbed sediment (Figure 3). Referring to the scanning results at large magnifications (from 1 μm to 10 μm) of London clay (Gasparre, 2005), we can obtain that the microstructure of Merville clay appears to be composed of aggregates of clayey particles.

An analysis of Merville clay minerals has been performed using X-ray diffractometer. The main minerals are quartz, illite and smectite, as well as kaolin as secondary element. High pressure one-dimensional compression tests on undisturbed samples have been performed in order to estimate the effective consolidation pressure, resulting in an OCR value larger than 20, as presented later on.

### 2.2 Test program

The tests performed in this study consist of one-dimensional consolidation tests and isotropically consolidated and undrained triaxial compression tests with pore water pressure measurement. Undisturbed samples of Merville clay from depths between 9 m and 11 m, where the mineralogy is assumed to be homogeneous, were prepared. In order to investigate the effect of the soil structure, reconstituted samples were also prepared. According to the method mentioned by Burland (1990), A mass of natural clay was first dried in an oven at 105°C, and then rolled into a powder state. The clay sample was reconstituted at a water

content of $w_L$ and 1. $5w_L$ (preferably $1.25w_L$) Thus, the powder was mixed with de-aired distilled water at a water content of $1.25w_L$ in this study, and the mixture was then consolidated under one-dimensional condition at a vertical stress $\sigma'_v$ of 100 kPa or 300 kPa. Consolidation was assumed to be fully attained when the axial displacement was smaller than 0.1 mm per day for an initial height of the specimens around 450 mm. The consolidation took at least three weeks, but the consolidation stage lasted finally one month to ensure the full saturation and the complete consolidation.

Three oedometer tests on undisturbed specimens, named Oed-$CRS_L$-I, Oed-$CRS_M$-I and Oed-$CRS_H$-I, were conducted. The specimens were 70 mm in diameter and 19 mm in height. Because the preconsolidation pressure is high, compared to the capacity of standard oedometer tests, tests under constant rate of strain (CRS), instead of conventional load-control tests, were carried out for estimating the rate-dependency on the preconsolidation pressure, using a load cell with a capacity of 50 kN. A CRS test on a reconstituted clay specimen (Oed-CRS-R) was also carried out for comparison. During loading, the drainage was permitted through the bottom and the top of the specimen. The axial strain rate used in the CRS loading tests varied from 0.13 %/h to 1.26 %/h. According to similar strain rate tests by Jia and Lei (2017) on the clay with plastic index (PI) more than 50, the excess pore-water pressure of the specimen during loading could be negligible. A standard load-control oedometer test with 24 h load stages on a reconstituted sample (Oed-Con-R) was also conducted up to a vertical effective stress of 700 kPa.

Undrained triaxial tests were conducted on undisturbed clay specimens with OCR=7, 14, 28 and 56, assuming an effective preconsolidation stress of 2800 kPa, as determined from the CSR oedometer tests (see next section). For comparison, undrained triaxial tests on reconstituted clay specimens with OCR=1, 7 and 14 were also conducted. The specimens for the triaxial tests were 35 mm in diameter and 70 mm in height according to the computer-controlled GDS triaxial testing system employed in this study. Three different axial strain rates were selected: 0.26 %/h, 2.57 %/h and 25.89 %/h, the strain-rate of 2.57 %/h being usually adopted in conventional undrained triaxial tests. A back pressure of 300 kPa was applied to all the specimens. The *B*-value was checked and found to be greater than 0.96

for all the tests. The undisturbed specimens were isotropically consolidated up to the target effective consolidation pressure (e.g., 100 or 300 kPa) by loading steps at the rate of 50 kPa/day, and the reconstituted specimens were isotropically consolidated to a higher effective stress kept constant for one week, followed by an unloading stage at the rate of ±50 kPa/day to the target effective consolidation pressure maintained constant for one day before shearing. After the isotropic consolidation stage, the cell pressure was kept constant and the specimen was sheared to failure under undrained condition at a constant axial strain rate with pore water pressure measurement at the bottom of the specimen. The degrees of saturation of all test specimens are above 99 %.

As mentioned above, the highest axial strain rate is about 25.89%/h. One possible problem is the redistribution of pore water pressure at this high strain rate of 25.89%/h relating to permeability. Lebbe et al (1991) have carried out tests on the clay from Flanders region and obtained the hydraulic conductivity of this clay equal to $3.2 \times 10^{-7}$ m/s. According to Yin and Hicher (2008), at a strain rate of 25.89%/h the problem of pore-water pressure redistribution inside of the specimen of Merville clay during shearing may be ignored. Moreover, the side strips were used to ensure that the possible small pore-water pressure redistribution being completed within a short period of time.

# 3 Test results and interpretation

## 3.1 One-dimensional compression behavior

Figures 4(a) and (b) show the results of one conventional oedometer test on a reconstituted clay specimen preconsolidated under a vertical pressure of 100 kPa. It can be used as a reference for comparison with the test results on undisturbed clay specimens and also for determining the intrinsic properties of the tested clay. The plastic compression index is measured as $\lambda = -\Delta e/\Delta \ln \sigma'_v = 0.155$, the swelling index $\kappa = -\Delta e/\Delta \ln \sigma'_v = 0.02$, and the secondary compression coefficient $C_{\alpha e} = -\Delta e/\Delta \ln t = 0.004$. The ratio $C_{\alpha e}/\lambda = C_\alpha/C_c = 0.026$ is close to values for inorganic silty clay according to Mesri and Castro (1987), which is consistent with Casagrande's classification for the tested clay.

To further study strain rate dependency, one high pressure CRS oedometer test on a

reconstituted clay specimen consolidated under a vertical pressure of 300 kPa was conducted (Figure 4(c)). For this CRS test, the strain-rate behavior appears similar to the isotach pattern. It is relatively easy to extrapolate parallel compression curves corresponding to each strain rate (in dotted lines) in Figure 4(d). The stresses at three points of the intersection between the first unloading line and the three dotted lines are considered as the apparent preconsolidation pressures. Thus, three apparent preconsolidation pressures relative to the first unloading-reloading cycle are measured for different strain rates, and plotted in a double-logarithm plane at the top right-hand corner in Figure 4(d). A linear relationship could be found in agreement with the expression suggested by Yin et al. (2010; 2011; 2014):

$$\frac{\left(\sigma_{p0}\right)_{\dot{\varepsilon}_v}}{\left(\sigma_{p0}\right)_{\dot{\varepsilon}_{v0}}}=\left(\frac{\dot{\varepsilon}_v}{\dot{\varepsilon}_{v0}}\right)^{1/\beta} \tag{1}$$

where $\left(\sigma_{p0}\right)_{\dot{\varepsilon}_v}$ is the preconsolidation pressure for a given vertical strain rate $\dot{\varepsilon}_v$; $\beta$ is the rate-dependency coefficient. The value of the rate-dependency parameter $\beta$ was found equal to 32.3. This value is close to $\beta = (\lambda\text{-}\kappa)/C_{\alpha e} = 33.7$ estimated by conventional oedometer tests following the idea of the uniqueness between rate-dependency and creep behavior (Yin et al., 2014). This relationship agrees with the hypothesis B (Yin 2015), and has been adopted in viscoplastic modeling of soft clays and finite element analysis of clay foundation (Yin et al. 2015).

Three oedometer tests at constant strain-rates of 0.13%/h, 0.63%/h and 1.26%/h have been performed on undisturbed specimens, as shown in Figure 5. The strain rate effect is very small at the beginning of the loading up to the preconsolidation pressure of about 2800 kPa obtained by the Casagrande's method. Comparing undisturbed specimens to reconstituted specimens in Figure 5(a), the inter-particle cementation related bonding ratio $\chi_0$, defined as the difference between the preconsolidation pressure of undisturbed specimen and the stress at the intersection point of the reconstituted and undisturbed compression curves divided by the stress at intersection (Yin et al., 2011), can be estimated as follows:

$$\chi_0 = (2800\text{-}445)/445=5.3 \text{ (detailed in Figure 5(a))} \tag{2}$$

The strain rate effect becomes more important for high stress levels (Figure 5(b)). The rate-dependency of natural clay is indeed clearly found, but its amplitude is difficult to estimate precisely in one-dimensional loading due to the natural variability of the undisturbed samples.

## 3.2 Undrained shear behavior for the adhesive bond shearing resistance

### *3.2.1 Triaxial tests of reconstituted specimens with different OCRs*

Since the natural clay has a very high preconsolidation pressure, and tests on low OCR samples are needed as reference, three series of undrained triaxial compression tests on reconstituted specimens with *OCR*=1, 7, and 14 are first performed, and are summarized in Table 3. For each OCR, three strain rates are applied on three identical reconstituted specimens.

Figure 6(a) shows the relationship between the deviatoric stress $q$ (equal to the difference between the axial effective stress and radial effective stress "$\sigma'_a$-$\sigma'_r$") and the axial strain $\varepsilon_a$ for normally consolidated specimens. The undrained shear strength increases with an increase in the strain rate. The figure also presents the changes in the excess pore water pressure $\Delta u$ with the axial strain during shearing. The effect of the strain rate on the induced excess pore water pressure is small. Figure 6(b) shows the stress paths in the ($p'$-$q$) plane, based on which the slope of the critical state line in compression $M_c$ = 1 (corresponding to a friction angle $\phi_c$ of 25.4º) is obtained, where the effective mean pressure $p'$ is equal to "$(\sigma'_a+2\sigma'_r)/3$".

Figures 6(c) to 6(f) present the relationships between the deviatoric stress and the axial strain, between the excess pore water pressure and the axial strain, and the stress paths in the ($p'$-$q$) plane for the test series with *OCR*=7 and 14. The strain rate effect on the deviatoric stress appears clearly. Similar to the tests at *OCR*=1, higher strain rates lead to higher undrained shear strengths. The pore water pressures in the *OCR*=7 and 14 test series firstly increase and then decrease with an increase in the axial strain. The stress paths obtained from the *OCR*=7 and 14 test series do not reach the critical state line, which can be obtained only at elevated axial strains. For OCR=14, a clear rupture of two specimens is observed during

undrained shearing.

To characterize the influence of the strain rate on the undrained shear behavior, Yin et al. (2011; 2015) suggested that the undrained shear strength varies almost linearly with the strain rate in a double logarithm plot, expressed as follows:

$$\frac{\left(q_{\mathrm{f}}/p_0'\right)_{\dot{\varepsilon}_a}}{\left(q_{\mathrm{f}}/p_0'\right)_{\dot{\varepsilon}_{a0}}}=\left(\frac{\dot{\varepsilon}_a}{\dot{\varepsilon}_{a0}}\right)^{1/\beta} \tag{3}$$

where $(q_{\mathrm{f}}/p_0')_{\dot{\varepsilon}_a}$ is the normalized undrained shear strength for a given strain rate $\dot{\varepsilon}_a$; $\beta$ is the rate-dependency coefficient based on the shear strength evolution and assumed to be identical to the rate-dependency coefficient on the preconsolidation pressure measured in the previous section. According to this idea, the normalized undrained shear strengths are plotted against the applied axial strain rate for all specimens with different OCRs (Figure 7). Three values of OCRs correspond to three lines, and the values of $1/\beta$ are 0.0345, 0.0337 and 0.0307, respectively. Based on these results, the rate-dependency for different OCRs can be considered as unique since the slope $1/\beta$ for different OCRs is almost the same. A mean value of $\beta$ = 30 could be estimated which is close to the one obtained from the oedometer tests (32.3 from CRS test and 33.7 from conventional test). This reveals that in viscoplastic modeling based on the overstress theory, it is true that a same rate-dependency parameter in overstress function can be applicable for different stress paths.

*3.2.2 Triaxial tests of undisturbed specimens with different OCRs*

Four series of undrained triaxial compression tests on undisturbed specimens with *OCR*=7, 14, 28, and 56 were performed (Han et al., 2014). Strain localization and a shear band formation have been observed in all specimens during shearing. For stress-strain response of overconsolidated clay, the post peak deformation is concentrated in a narrow zone that is called shear band. This phenomenon, i.e. concentration of irreversible deformation in a zone with a limited thickness, is known as strain localization or localization of deformation (Hicher et al., 1997). Table 4 presents the results of all the tests in terms of effective consolidation pressure $p'_0$, *OCR*, inclination of shear band to horizontal direction,

stress-strain properties and pore water pressure increase at the maximum deviatoric stress (failure), and maximum excess pore water pressure during shearing.

It is found that, for each test, the axial strain at the maximum excess pore water pressure $\varepsilon_{uf}$ is smaller than the axial strain at the peak stress $\varepsilon_f$, which means that the maximum excess pore water pressure $\Delta u_m$ is reached sooner than the peak shear stress $q_f$, which shows that the phase transformation state from contraction to dilation occurred before the peak stress state. The same phenomenon was observed for London clay by Bishop et al. (1965). The observed angle of shear band with the horizontal direction varies from 54° to 68° for all samples with a mean value of 63°, close to the theoretical angle ($\pi/4+\phi_c/2$ = 57.7°) estimated from the critical state friction angle measured on the reconstituted clay.

Figure 8 presents the relationship between the deviatoric stress and the axial strain, between the excess pore water pressure and the axial strain, and the stress paths in the ($p'$-$q$) plane for all tests on samples. For all tests, a higher strain rate leads to a higher undrained shear strength. Concerning the evolution of the pore water pressure, the three curves are almost identical before reaching the maximum pore water pressure, which means that the evolution of the pore water pressure is almost independent of the strain rate before the maximum pore water pressure in this heavily overconsolidated stiff clay was obtained.

As done previously for the reconstituted specimens, the normalized undrained shear strengths are plotted against the applied axial strain rate for all undisturbed specimens with different OCRs (Figure 9(a)). In Figure 9(a), four values of OCRs correspond to four lines, and the values of $1/\beta$ are 0.0428, 0.0479, 0.0429 and 0.045, respectively. Thus, a mean value of $\beta$ = 22.4 could be estimated. Comparing the slope $1/\beta$ in Figures 7 and 9, the slope of undisturbed specimens is greater than that of reconstituted specimens, which indicates a larger rate-dependency in comparison to reconstituted clay. This higher rate-dependency can be explained by the inter-particle bonding formed during the geological history. For obtaining the cohesion according to Mohr-Coulomb theory, the curves of test results are re-plotted in the plane of $(\sigma'_1+\sigma'_3)/2$ and $(\sigma'_1-\sigma'_3)/2$ in Figures 9(b) and (c). As shown for specimens with OCR=7 in Figure 9(b), the difference between the cohesion of undisturbed specimen and that of reconstituted specimen with the same OCR is named as the additional cohesion $\Delta c$. This is

due to inter-particle bonding and can be measured for different strain rates by comparing results of reconstituted and undisturbed clays, assuming that the critical friction angle does not depend on inter-particle bonds. Note that the apparent cohesion of reconstituted specimens is contributed by the overconsolidation relating to the so-called Hvorslev envelope instead of inter-particle adhesive bonds. The same interpretation can be made for specimens with OCR=14 (Figure 9(c)). Then, this additional cohesion, called the adhesive bond shearing resistance and expressed as $c'_{ad}$, can be plotted versus the strain rate in a double log plane, assuming a correlation of the same form as Equation (1) (see Figure 9(d)).

$$\frac{\left(c'_{ad}\right)_{\dot{\varepsilon}_a}}{\left(c'_{ad}\right)_{\dot{\varepsilon}_{a0}}} = \left(\frac{\dot{\varepsilon}_a}{\dot{\varepsilon}_{a0}}\right)^{1/\beta'} \tag{4}$$

Then, the strain rate influence on the adhesive bond shearing resistance is estimated with the coefficient $\beta'$ which is found equal to 12. This smaller value of $\beta'$ compared to two values of $\beta$ for Merville clay indicates that the influence of the inter-particle bonding results in a larger overall rate-dependency of the undrained shear strength for undisturbed clay. The Eq.(4) can be a fundamental relation for extending the time-dependent modeling of stiff clay to include the shear mechanism of rate-dependent adhesive bonding, similar to compression mechanism of inter-particle bonding for soft soils (Yin et al., 2011, 2017; Zhu et al., 2016).

This difference in strain rate-dependency between undisturbed clay and reconstituted clay is due to inter-particle bonding. It is consistent with the research conclusion of London clay, that is to say, the natural structure in London clay is responsible for the different strain-rate-related behaviours of the undisturbed and reconstituted overconsolidated samples (Sorensen et al., 2007). Thus, it is reasonable to assume that the inter-particle debonding of undisturbed clay specimens during shearing is also rate-dependent. Indeed, the debonding is due to a progressive damage of the inter-aggregates bonds. This damage depends on the macroscopic strains experienced by the specimen. At a given stress level, the strain amplitude decreases with the increase of the strain rate and, therefore, the amplitude of damage also decreases. Note that this could be further examined by advanced x-ray nano-CT scan technique using a small specimen with loading applied.

## 4 Conclusions

Both reconstituted and undisturbed overconsolidated samples with different overconsolidation ratios on Merville clay were prepared. They are submitted to a series of oedometer and undrained triaxial tests under different confining stresses with different strain rates, covering a range of OCRs up to 56. The influence of both the strain rate and the OCR on the undrained strength is analyzed, and the comparison is carried out between undisturbed and reconstituted specimens to approach the strain rate dependency of the adhesive bond shearing resistance.

Under undrained triaxial loading, the rate-dependency for reconstituted clay with different OCRs can be considered as unique since the parameter $\beta$ based on the normalized undrained shear strength versus the strain rate is almost the same for different OCRs, with a mean value of 30 close to the one obtained from oedometer tests. For reconstituted clay, the uniqueness of the rate-dependency under one-dimensional and triaxial conditions with different OCRs is obtained. In parallel, the rate-dependency of undisturbed clay for different OCRs from 7 to 56 can be considered as unique with a mean value of $\beta = 22.4$. The effect of inter-particle bonding was investigated by comparing the tests on undisturbed and reconstituted specimens with the same OCRs (7 and 14). The results suggest that the higher rate-dependency for undisturbed clay compared to reconstituted clay is due to the rate-dependency of inter-particle debonding in undisturbed clay specimens. This new finding is formulated (see Eq.(4)) as the adhesive bond shearing resistance against the strain rate, which should be useful for improving the time-dependent modeling of highly overconsolidated stiff clays.

## Acknowledgment

The financial supports provided by a PROCORE-France/Hong Kong Joint Research Project (F-PolyU501/19) from Research Grants Council (RGC) of Hong Kong are gratefully acknowledged.

# References


[1] Ali H., Reiffsteck P., Baguelin F., et al. Settlement of pile using cone loading test: load settlement curve approach. CPT 10: 2nd Int. Symp. on Cone Penetration Testing, 2010, France.

[2] Bishop AW, Webb DL, Lewin PI. Undisturbed samples of London Clay from Ashford Common shaft: strength effective stress relationship. Géotechnique, 1965, 15(1), 1–31.

[3] Burland JB. On the compressibility and shear strength of natural soils. Géotechnique, 1990, 40(3), 329-378.

[4] Canépa Y, Borel S, Deconinck J. Determination of the degradation curve of the shear modulus of a soil from field tests. Paramètres de calcul géotechnique, Magnan, ENPC/LCPS press, Paris, 2002, 25-32.

[5] D'Onofrio, A, Silvestri D, Vinale F. Strain rate dependent behavior of a natural stiff clay. Soils Found., 1999, 39(2), 69-82.

[6] Ferber V, Abraham O. Contribution of the seismic methods to the determination of initial moduli: application on the experimental site of Merville. Paramètres de calcul géotechnique. Magnan, ENPC/LCPS press, Paris, 2002, 41-48.

[7] Gasparre A. Advanced laboratory characterisation of London clay. PhD Thesis, 2005, Imperial College London.

[8] Graham J, Crooks JHA, Bell AL. Time effects on the stress-strain behaviour of natural soft clays. Géotechnique, 1983, 33(3), 327-340.

[9] Gu LL, Wang Z, Huang Q, et al. Numerical investigation into ground treatment to mitigate the permanent train-induced deformation of pile-raft-soft soil system. Transp. Geotech., 2020, doi: 10.1016/j.trgeo.2020.100368.

[10] Han J, Dano C, Hicher PY, et al. Strain-rate dependency of shear strength for a highly overconsolidated clay. Int. Conf. Geo-Shanghai, 2014(236), 343-352.

[11] Hicher PY, Wahyudi H, Tessier D. Microstructural analysis of strain localization in clay.

359 Comput. Geotech., 1997, 16, 205-222.

360 [12] Hieng IO. Loi de comportement d'une argile raide (détermination des paramètres
361 géotechniques de l'argile des Flandres). PhD Thesis, 1991, University Paris VI (in
362 French).

363 [13] Indraratna B, Korkitsuntornsan W, Nguyen TT. Influence of Kaolin content on the cyclic
364 loading response of railway subgrade. Transp. Geotech., 2020, doi:
365 10.1016/j.trgeo.2020.100319.

366 [14] Jia R, Lei HY. Effect of strain rate on consolidation behavior of Ariake clay and
367 selection of the suitable strain rate. Chinese Journal of Geotechnical Engineering, 2017,
368 39(Supp.2), 198-202 (in Chinese).

369 [15] Josseaume H. Engineering properties of the Flanders clay at Dunkerque and Calais.
370 Revue Française de Géotechnique, 1998, 84, 3-26.

371 [16] Josseaume H, Hieng IO, Stempfelet JP. Détermination des paramètres de compressibilité
372 d'une argile raide à partir d'essais oedométriques à haute pression. Bulletin de LCPC,
373 1991, 109-120 (in French).

374 [17] Karstunen M, Yin ZY. Modelling time-dependent behaviour of Murro test embankment.
375 Géotechnique, 2010, 60(10), 735-749.

376 [18] Lebbe L, Mahauden M, De Breuck W. Interpretation of pumping tests in the anisotropic
377 Brabant Massif by means of a numerical inverse model. Annales de la Société
378 Géologique de Belgique, 1991, 114(1), 277-282.

379 [19] Mesri G, Castro A. Cα/Cc concept and K0 during secondary compression. J. Geotech.
380 Eng., 1987, 113(3), 230-247.

381 [20] Sheahan TC, Ladd CC, Germaine JT. Rate-dependent undrained shear behavior of
382 saturated clay. J. Geotech. Geoenviron. Eng., 1996, 122(2), 99-108.

383 [21] Sorensen KK, Baudet BA, Simpson B. Influence of structure on the time-dependent
384 behaviour of a stiff sedimentary clay. Géotechnique, 2007, 57(1), 113-124.

385 [22] Tavenas F, Leroueil S. Effect of stresses and time on yielding of clays. Proc., 9th Int.

386 Conf. on Soil Mechanics and Foundation Engineering, Tokyo, 1977, 1, 319-326.

387 [23] Vaid YP, Robertson PK, Campanella RG. Strain rate behavior of Saint-Jean-Vianney clay.
388 Can. Geotech. J., 1979, 16(1), 34-42.

389 [24] Yang J, Yin ZY, Liu XF, et al. Numerical analysis for the role of soil properties to the
390 load transfer in clay foundation due to the traffic load of the metro tunnel. Transp.
391 Geotech., 2020, 23: 100336.

392 [25] Yao YP, Hou W, Zhou AN. UH model: three-dimensional unified hardening model for
393 overconsolidated clays. Géotechnique, *2*009, 59(5), 451-469.

394 [26] Yao YP, Huang J, Wang ND, et al. Prediction method of creep settlement considering
395 abrupt factors. Transp. Geotech., 2019, doi: 10.1016/j.trgeo.2019.100304.

396 [27] Yao YP, Kong LM, Zhou AN. Time-dependent unified hardening model:
397 three-dimensional elasto-visco-plastic constitutive model for clays. J. Eng. Mech., 2015,
398 141(6), 0414162.

399 [28] Yin JH. Fundamental Issues of Elastic Viscoplastic Modeling of the Time-Dependent
400 Stress–Strain Behavior of Geomaterials. Int. J. Geomech. ASCE, 2015, 15(5):
401 A4015002.

402 [29] Yin Z-Y, Xu Q, Yu C. Elastic viscoplastic modeling for natural soft clays considering
403 nonlinear creep. Int. J. Geomech. ASCE, 2015, 15(5): A6014001.

404 [30] Yin ZY, Chang CS, Karstunen M, et al. An anisotropic elastic viscoplastic model for soft
405 clays. Int. J. Solids Struct., 2010, 47(5), 665-677.

406 [31] Yin ZY, Hicher PY. Identifying parameters controlling soil delayed behaviour from
407 laboratory and in situ pressuremeter testing. Int. J. Numer. Anal. Meth. Geomech., 2008,
408 32(12), 1515-1535.

409 [32] Yin ZY, Karstunen M, Chang CS, et al. Modeling time-dependent behavior of soft
410 sensitive clay. J. Geotech. Geoenviron. Eng., 2011, 137(11), 1103-1113.

411 [33] Yin ZY, Yin JH, Huang HW. Rate-dependent and long-term yield stress and strength of
412 soft Wenzhou marine clay: experiments and modeling. Mar. Georesour. Geotech., 2015,

413 33(1), 79-91.

414 [34] Yin ZY, Zhu QY, Yin JH, et al. Stress relaxation coefficient and formulation for soft soils.
415 Géotechnique Letters, 2014, 4(1), 45-51.

416 [35] Yin ZY, Zhu QY, Zhang DM. Comparison of two creep degradation modeling
417 approaches for soft structured soils. Acta Geotech., 2017, 12(6), 1395–1413.

418 [36] Zhu QY, Yin ZY, Hicher PY, Shen SL. Nonlinearity of one-dimensional creep
419 characteristics of soft clays. Acta Geotech., 2016, 11(4), 887-900.

420 [37] Zhu JG, Yin JH. Strain-rate-dependent stress-strain behavior of overconsolidated Hong
421 Kong marine clay. Can. Geotech. J., 2000, 37(6), 1272-1282.

# Tables

**Table 1.** Physical properties of tested Merville stiff clay

| | |
|---|---|
| Liquid limit (%) | 97.2±2.0 |
| Plastic limit (%) | 40.5±2.0 |
| Plasticity index PI | 59.0±1.0 |
| Natural water content (%) | 30.2±1.5 |
| Degree of saturation (%) | 100 |
| Specific weight (kN/m$^3$) | 19.5 |
| Specific gravity of solids | 2.67±0.2 |
| Percent finer than 2 μm (%) | 26 |
| Activity PI/(% < 2 μm) | 2.25±0.08 |

426 **Table 2.** List of oedometer and triaxial tests on 9-11 m Merville clay specimens

| Test | Maximum effective stress during consolidation (kPa) | $e_0$ of initial sample | Confining stress (kPa) | Strain-rate (%/h) |
|---|---|---|---|---|
| Oed-Con-R | 100 | 1.223 | - | - |
| Oed-CRS-R | 300 | 0.959 | - | 0.13/0.63/1.26 |
| Oed-$CRS_L$-I | - | 0.756 | - | 0.13 |
| Oed-$CRS_M$-I | - | 0.757 | - | 0.63 |
| Oed-$CRS_H$-I | - | 0.757 | - | 1.26 |
| Tri-$CRS_L$-OCR1-R | 100 | 1.223 | 100 | 0.26 |
| Tri-$CRS_M$-OCR1-R | 100 | 1.223 | 100 | 2.57 |
| Tri-$CRS_H$-OCR1-R | 100 | 1.223 | 100 | 25.89 |
| Tri-$CRS_L$-OCR7-R | 700 | 1.223 | 100 | 0.26 |
| Tri-$CRS_M$-OCR7-R | 700 | 1.223 | 100 | 2.57 |
| Tri-$CRS_H$-OCR7-R | 700 | 1.223 | 100 | 25.89 |
| Tri-$CRS_L$-OCR14-R | 700 | 1.223 | 50 | 0.26 |
| Tri-$CRS_M$-OCR14-R | 700 | 1.223 | 50 | 2.57 |
| Tri-$CRS_H$-OCR14-R | 700 | 1.223 | 50 | 25.89 |
| Tri-$CRS_L$-OCR7-I | - | 0.742 | 400 | 0.26 |
| Tri-$CRS_M$-OCR7-I | - | 0.745 | 400 | 2.57 |
| Tri-$CRS_H$-OCR7-I | - | 0.742 | 400 | 25.89 |
| Tri-$CRS_L$-OCR14-I | - | 0.739 | 200 | 0.26 |
| Tri-$CRS_M$-OCR14-I | - | 0.743 | 200 | 2.57 |
| Tri-$CRS_H$-OCR14-I | - | 0.745 | 200 | 25.89 |
| Tri-$CRS_L$-OCR28-I | - | 0.745 | 100 | 0.26 |
| Tri-$CRS_M$-OCR28-I | - | 0.745 | 100 | 2.57 |
| Tri-$CRS_H$-OCR28-I | - | 0.743 | 100 | 25.89 |
| Tri-$CRS_L$-OCR56-I | - | 0.740 | 50 | 0.26 |
| Tri-$CRS_M$-OCR56-I | - | 0.745 | 50 | 2.57 |
| Tri-$CRS_H$-OCR56-I | - | 0.743 | 50 | 25.89 |

427 Remarks: Oed-oedometer test, Con-conventional loading, R-reconstituted sample, I-undisturbed
428 sample; Tri-triaxial test, CRS-constant rate of strain, _L-low strain rate, _M-medium strain rate,
429 _H-high strain rate, OCRxx-overconsolidation ratio of xx.

**Table 3.** Test results on reconstituted specimens at different strain rates

| Test | $p'_{max}$ (kPa) | $e_1$ | $p'_0$ (kPa) | $e_2$ | OCR | Strain rate (%/h) | $\varepsilon_f$ (%) | $q_f$ (kPa) | $\Delta u_f$ (kPa) |
|---|---|---|---|---|---|---|---|---|---|
| Tri-$CRS_L$-OCR1-R | 99.1 | 1.282 | 99.1 | 1.282 | 1.0 | 0.26 | 4.75 | 85.3 | 37.3 |
| Tri-$CRS_M$-OCR1-R | 100.1 | | 100.1 | | 1.0 | 2.57 | 4.52 | 89.1 | 42.0 |
| Tri-$CRS_H$-OCR1-R | 99.6 | | 99.6 | | 1.0 | 25.89 | 4.27 | 92.3 | 40.5 |
| Tri-$CRS_L$-OCR7-R | 699.8 | 0.742 | 99.0 | 0.848 | 7.1 | 0.26 | 6.04 | 183.5 | 22.5 |
| Tri-$CRS_M$-OCR7-R | 697.0 | | 100.2 | | 7.0 | 2.57 | 5.79 | 197.5 | 32.5 |
| Tri-$CRS_H$-OCR7-R | 701.0 | | 99.7 | | 7.0 | 25.89 | 5.64 | 219.6 | 33.3 |
| Tri-$CRS_L$-OCR14-R | 700.3 | | 50.7 | 0.886 | 13.8 | 0.26 | 4.87 | 121.3 | 15.2 |
| Tri-$CRS_M$-OCR14-R | 699.1 | | 49.7 | | 14.1 | 2.57 | 4.88 | 134.9 | 10.5 |
| Tri-$CRS_H$-OCR14-R | 699.0 | | 49.8 | | 14.0 | 25.89 | 7.61 | 154.1 | 9.2 |

Remarks: $p'_{max}$ is the maximum applied stress during consolidation stage; $p'_0$ is the final applied stress during consolidation stage; $e_1$ is the void ratio at the maximum applied stress of consolidation; $e_2$ is the void ratio at the final applied stress of consolidation (before shearing); $\varepsilon_f$ and $\Delta u_f$ are the axial strain and excess pore water pressure at the peak strength $q_f$.

437 **Table 4.** Test results on natural undisturbed specimens at different strain rates

| Test | $p'_0$ (kPa) | OCR | Strain rate (%/h) | $\varepsilon_f$ (%) | Angle α (°) | $q_f$ (kPa) | $\Delta u_f$ (kPa) | $\varepsilon_{uf}$ (%) | $\Delta u_m$ (kPa) |
|---|---|---|---|---|---|---|---|---|---|
| Tri-$CRS_L$-OCR7-I | 401.4 | 7.0 | 0.26 | 2.61 | 61 | 631.2 | 164.0 | 2.31 | 168.1 |
| Tri-$CRS_M$-OCR7-I | 399.8 | 7.0 | 2.57 | 3.14 | 64 | 690.2 | 160.3 | 2.54 | 167.9 |
| Tri-$CRS_H$-OCR7-I | 400.1 | 7.0 | 25.89 | 3.64 | 64 | 768.8 | 185.2 | 3.06 | 194.2 |
| Tri-$CRS_L$-OCR14-I | 199.3 | 14.0 | 0.26 | 3.49 | 64 | 426.6 | 107.2 | 2.99 | 117.2 |
| Tri-$CRS_M$-OCR14-I | 200.3 | 14.0 | 2.57 | 3.33 | 64 | 484.0 | 116.3 | 3.09 | 117.3 |
| Tri-$CRS_H$-OCR14-I | 200.1 | 14.0 | 25.89 | 3.70 | 61 | 532.3 | 113.9 | 3.30 | 116.4 |
| Tri-$CRS_L$-OCR28-I | 100.3 | 27.9 | 0.26 | 3.19 | 68 | 373.6 | 64.3 | 2.37 | 81.6 |
| Tri-$CRS_M$-OCR28-I | 100.8 | 27.8 | 2.57 | 2.96 | 63 | 415.3 | 80.7 | 2.47 | 88.8 |
| Tri-$CRS_H$-OCR28-I | 99.4 | 28.1 | 25.89 | 3.10 | 65 | 455.2 | 74.0 | 2.61 | 78.1 |
| Tri-$CRS_L$-OCR56-I | 50.8 | 55.1 | 0.26 | 2.92 | 61 | 312.4 | 35.0 | 1.60 | 41.0 |
| Tri-$CRS_M$-OCR56-I | 49.9 | 56.1 | 2.57 | 2.50 | 54 | 336.6 | 34.1 | 1.55 | 37.2 |
| Tri-$CRS_H$-OCR56-I | 49.3 | 56.8 | 25.89 | 2.69 | 58 | 383.3 | 31.2 | 2.13 | 36.9 |

438

439

## List of Figures

**Figure 1**

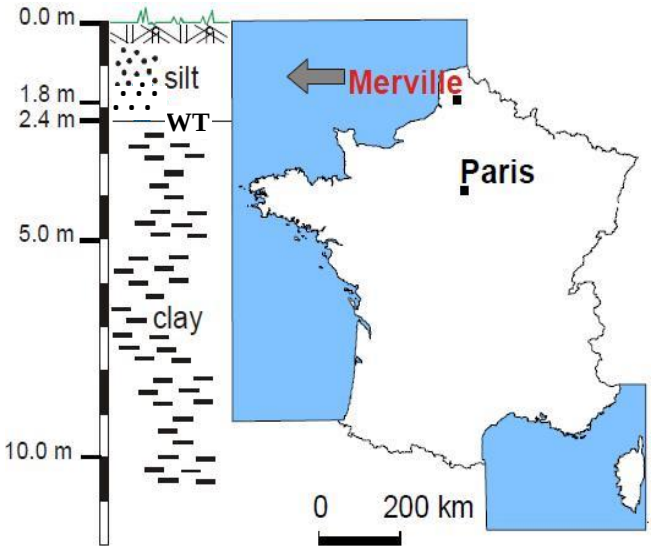

**Figure 2**

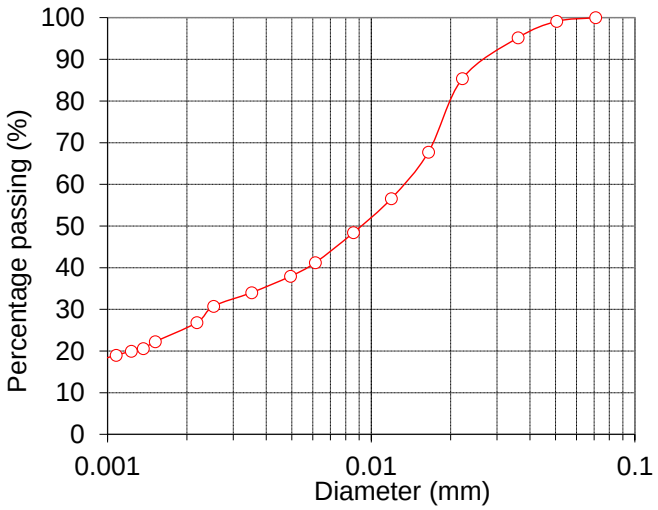
100
90
80
70
60
50
40
30
20
10
0
Percentage passing (%)
0.001
0.01
0.1
Diameter (mm)

**Figure 3**

(a) 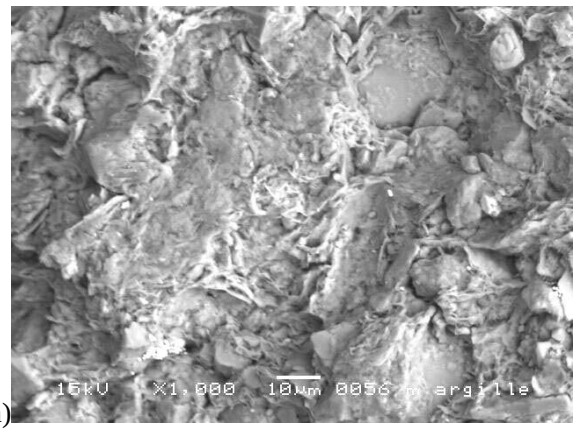


(b) 

**Figure 4**

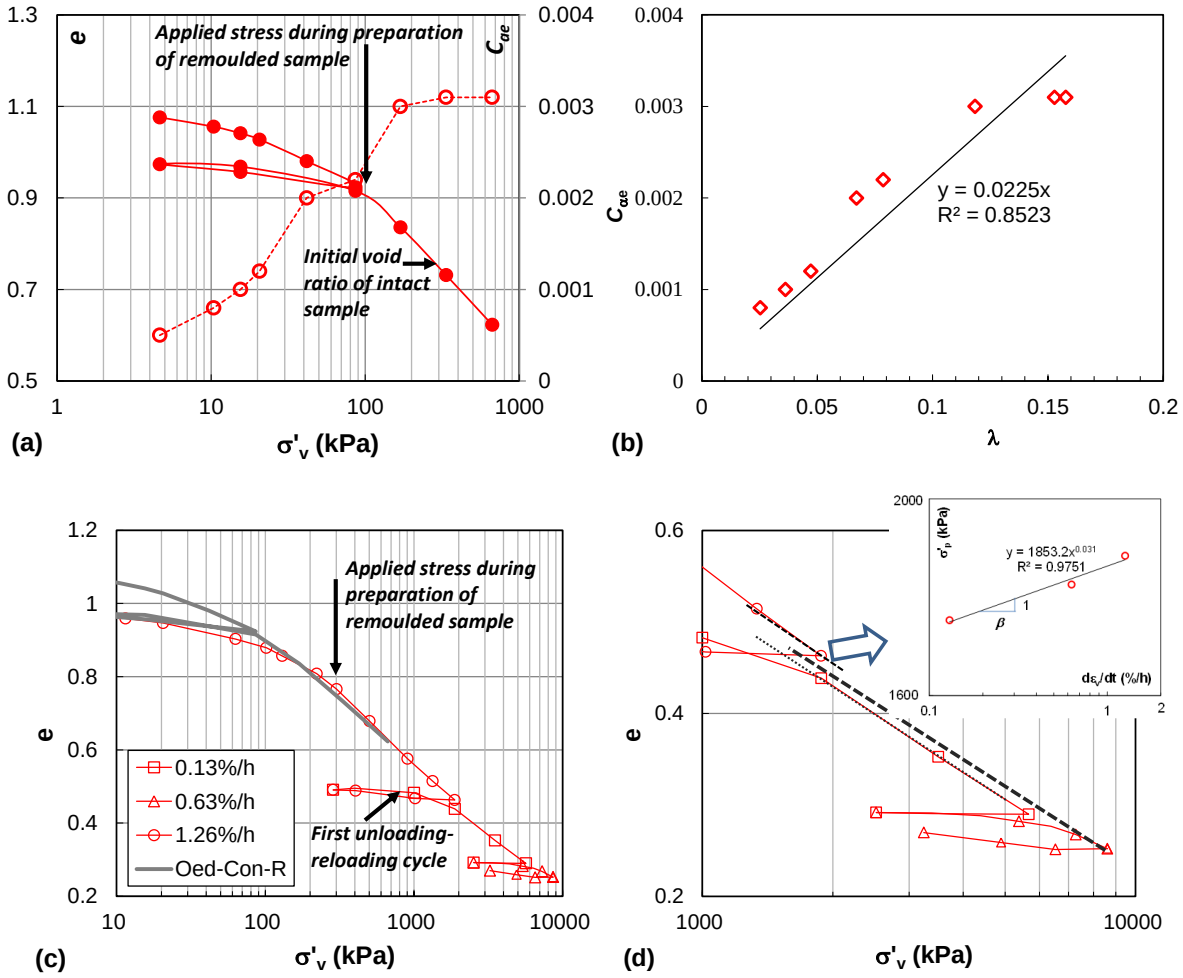
e
$C_{\alpha e}$
Applied stress during preparation of remoulded sample
Initial void ratio of intact sample
(a)
σ'v (kPa)
y = 0.0225x
R² = 0.8523
λ
(b)
Applied stress during preparation of remoulded sample
0.13%/h
0.63%/h
1.26%/h
Oed-Con-R
First unloading-reloading cycle
(c)
σ'v (kPa)
y = 1853.2x^0.031
R² = 0.9751
β
dεv/dt (%/h)
(d)
σ'v (kPa)

**Figure 5**

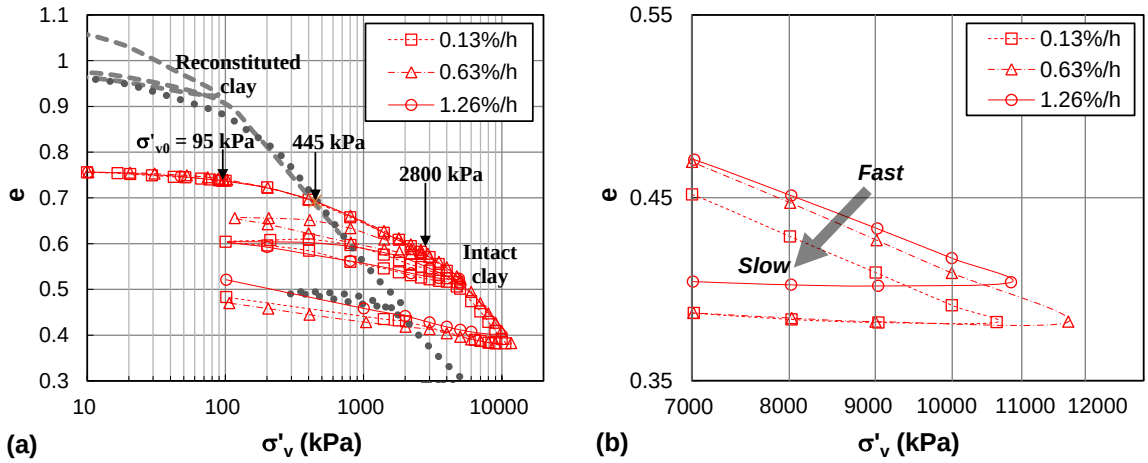
1.1
1
0.9
0.8
0.7
0.6
0.5
0.4
0.3
e
10
100
1000
10000
σ'v (kPa)
(a)
0.13%/h
0.63%/h
1.26%/h
Reconstituted clay
σ'v0 = 95 kPa
445 kPa
2800 kPa
Intact clay
0.55
0.45
0.35
7000
8000
9000
10000
11000
12000
(b)
Fast
Slow

**Figure 6**

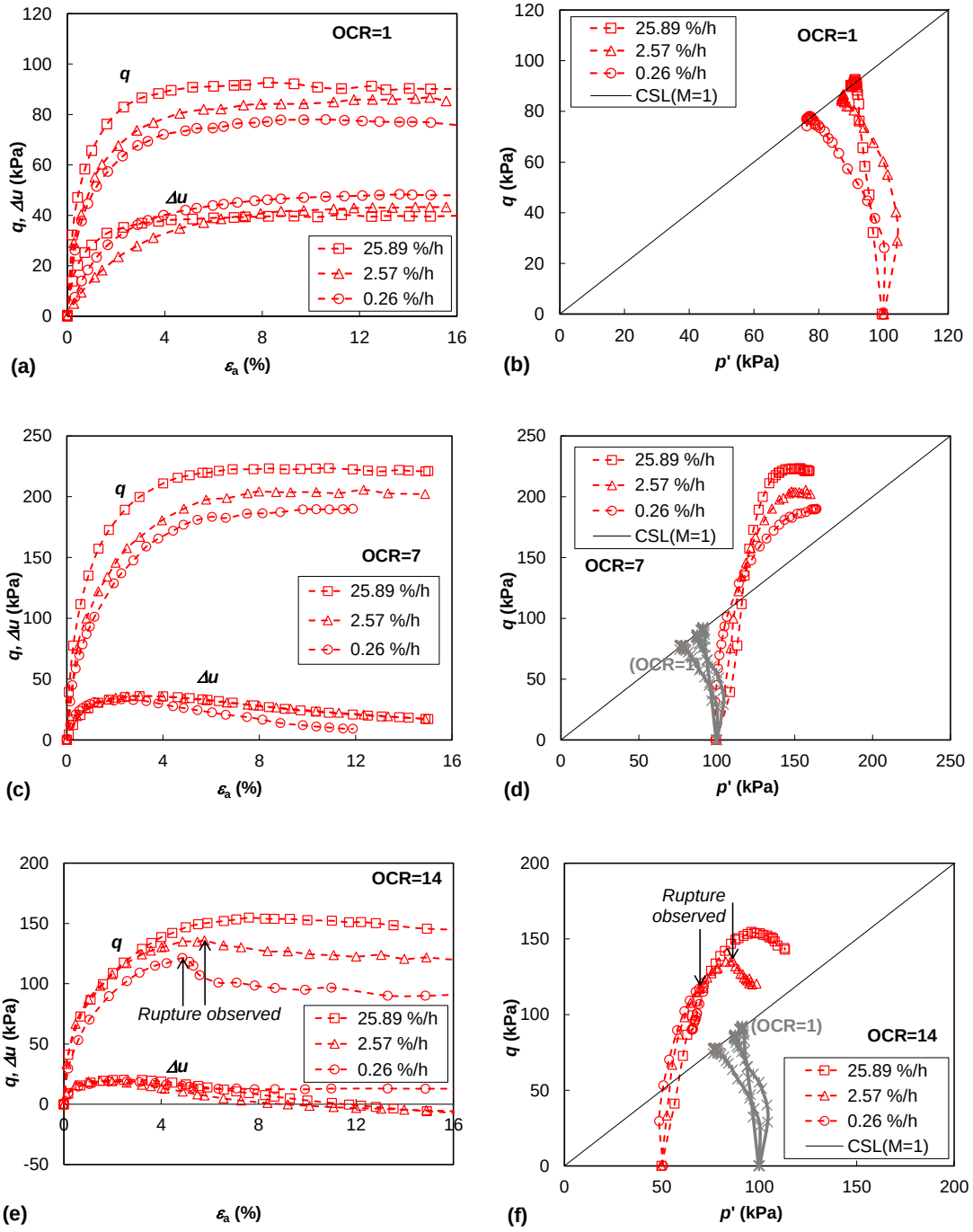
OCR=1
q
Δu
25.89 %/h
2.57 %/h
0.26 %/h
q, Δu (kPa)
εa (%)
(a)
CSL(M=1)
q (kPa)
p' (kPa)
(b)
OCR=7
(c)
(d)
(OCR=1)
OCR=14
Rupture observed
(e)
(f)

**Figure 7**

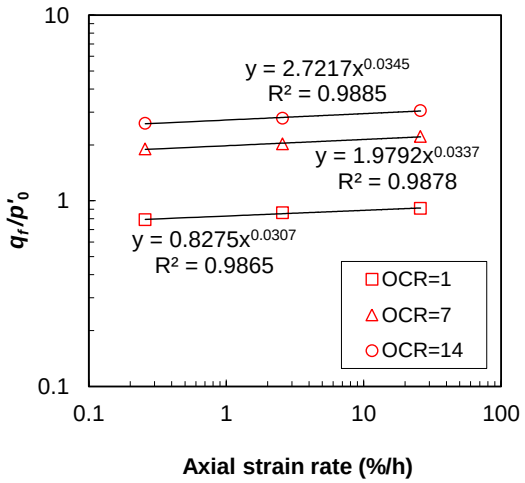
10
1
0.1
0.1
1
10
100
$q_f/p'_0$
Axial strain rate (%/h)
y = 2.7217x^0.0345
R² = 0.9885
y = 1.9792x^0.0337
R² = 0.9878
y = 0.8275x^0.0307
R² = 0.9865
OCR=1
OCR=7
OCR=14

**Figure 8**

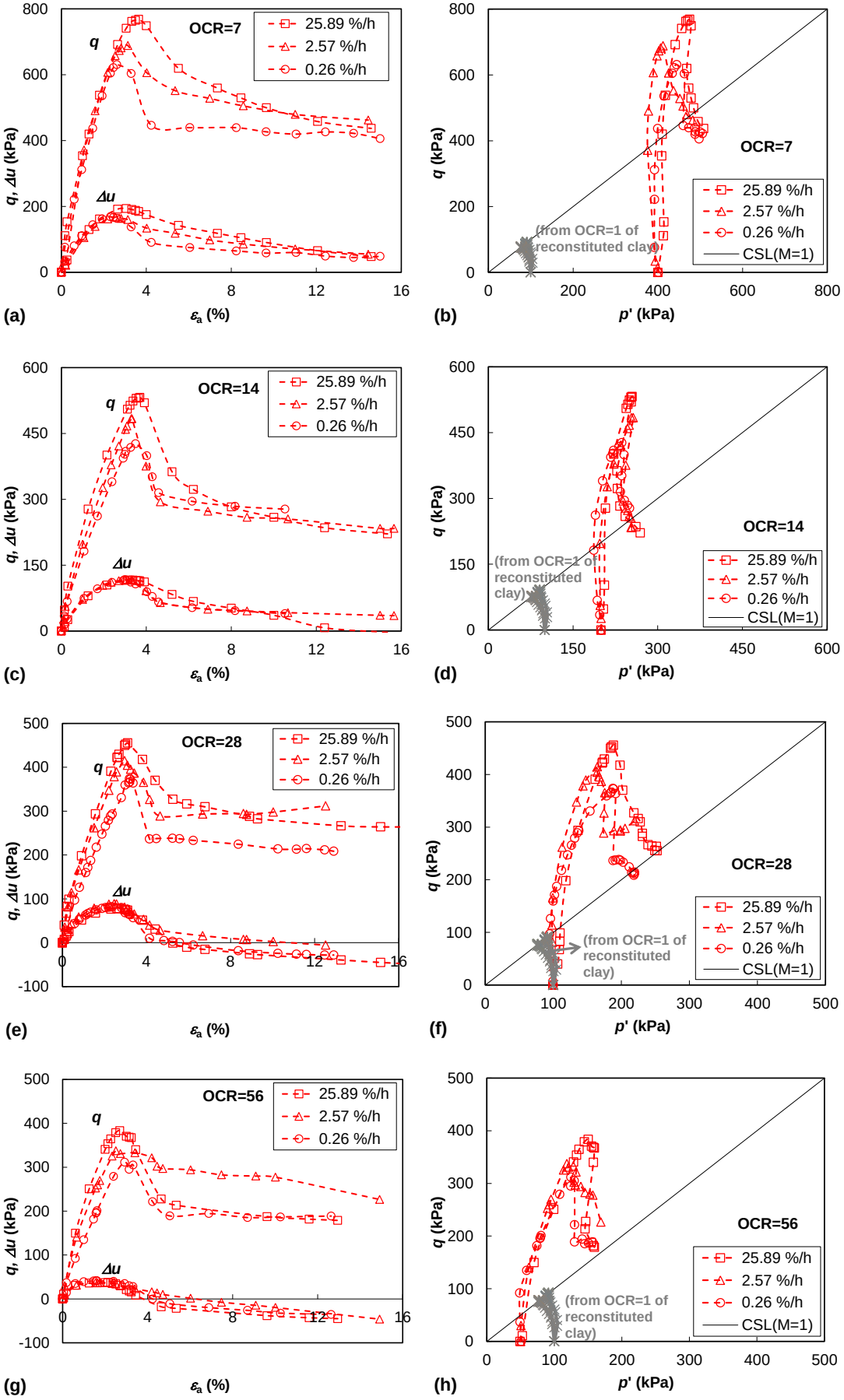
OCR=7
25.89 %/h
2.57 %/h
0.26 %/h
q
Δu
q, Δu (kPa)
εa (%)
(a)
q (kPa)
p' (kPa)
CSL(M=1)
(from OCR=1 of reconstituted clay)
(b)
OCR=14
(c)
(d)
OCR=28
(e)
(f)
OCR=56
(g)
(h)

**Figure 9**

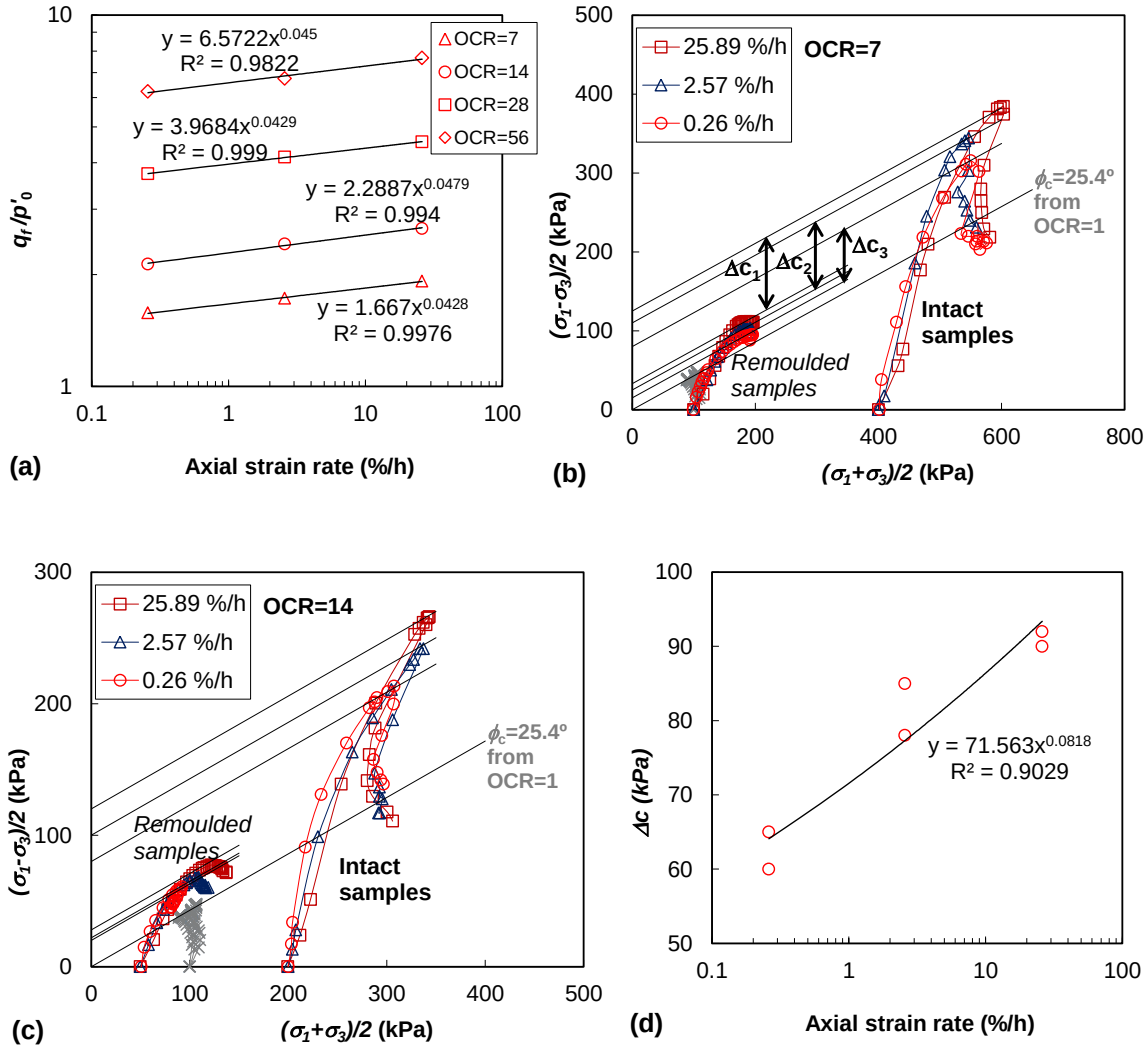
y = 6.5722x^0.045
R² = 0.9822
y = 3.9684x^0.0429
R² = 0.999
y = 2.2887x^0.0479
R² = 0.994
y = 1.667x^0.0428
R² = 0.9976
OCR=7
OCR=14
OCR=28
OCR=56
qt/p'0
Axial strain rate (%/h)
(a)
25.89 %/h
2.57 %/h
0.26 %/h
OCR=7
Δc1
Δc2
Δc3
Remoulded samples
Intact samples
ϕc=25.4° from OCR=1
(σ1-σ3)/2 (kPa)
(σ1+σ3)/2 (kPa)
(b)
OCR=14
(c)
y = 71.563x^0.0818
R² = 0.9029
Δc (kPa)
(d)